Solar Energy 159 (2018) 742–750

Contents lists available at ScienceDirect

Solar Energy

journal homepage: www.elsevier.com/locate/solener

Energy and exergy analyses of photovoltaic thermal collector with ∇-groove

Ahmad Fudholi*, Muhammad Zohri, Goh Li Jin, Adnan Ibrahim, Chan Hoy Yen, Mohd Yusof Othman, Mohd Hafidz Ruslan, Kamaruzzaman Sopian

Solar Energy Research Institute, Universiti Kebangsaan Malaysia, 43600 Bangi, Selangor, Malaysia

ARTICLE INFO

Keywords:
Mathematical model
Energy analysis
Exergy analysis
Improvement potential

ABSTRACT

Steady-state energy analysis was performed on a photovoltaic thermal (PVT) collector with ∇-groove. Energy balance equation was obtained using the analytical and the matrix inversion methods. Theoretical results were consistent with the experiments results. Theoretical and experimental studies were conducted under solar radiations of 385 and 820 W/m^2 and mass flow rates between 0.007 and 0.07 kg/s. Exergy analysis was performed to determine the effect of various solar radiations (300–1200 W/m^2). On the other hand, exergy analysis was performed to obtain loss exergy, PVT exergy efficiency, and improvement potential under solar radiations of 385 and 820 W/m^2 and mass flow rates between 0.007 and 0.07 kg/s.

1. Introduction

The twentieth century has been dubbed as the “hydrocarbon century” because of its wealth of hydrocarbons and its contribution to human development. Fossil fuels were formed over millions of years ago through the decay and decomposition of animals and plants under pressure and high temperature. Fossil fuels are vital to developed countries. Fossil fuels obtained underground and under the sea generate electricity. Fossil fuel combustion has contributed to the development of basic and continuous innovation. Approximately 90% of the world’s electricity production is from fossil fuel combustion (Greenhalgh, 2002).

The application of fossil fuels (coal, petroleum, and natural gas) is extensive. Specifically, petroleum is considered the most valuable resource in the development of human life. Petroleum is a dark and dense liquid; it is also called black gold. It is usually composed of various hydrocarbon compounds, including alkane series, and is usually found at the top of the crust. Petroleum is a primary energy source of vehicles. Aside from its use as fuel and lubricants, petroleum is also used in the manufacture of various products, such as solvents, fertilizers and pesticides, soaps and detergents, fragrances, plastics, and explosives. Pollution and damage caused by fossil fuel combustion include water pollution, air pollution, increased waste generation, soil depletion, and increased variety of human diseases. The influence of fossil fuel combustion on pollution and deterioration is extensive and difficult to gauge. The extinction of some aquatic species is among such effects. Carbon dioxide emissions largely contribute to the greenhouse effect. The increase in the greenhouse effect will increase the heat trapped in the Earth’s atmosphere and affect numerous areas. In Antarctica, the increase in the greenhouse effect and the heat causes melting of large ice chunks and lead to an increase in the seabed. Air pollution is another serious manmade problem in the atmosphere. Burning of fossil fuels causes carbon emissions and dust, and the dust will form a haze when it rises to a certain level. Haze is harmful to both human health and plant life. Nitrous oxide is released when coal is burned. The released nitrous oxide will be trapped in the atmosphere for a long time. Its effects on human health will be detected only after a long time.

Energy production from fossil fuels will also produce a considerable amount of waste material. Waste materials are waste products and toxic substances that are harmful to human health and the environment. Thus, thorough and detailed treatment or handling of waste materials is necessary to prevent the release of toxic substances to the environment. Maltreatment and mishandling will lead to its free release to land or water. Hence, humans, plants, and aquatic life will be directly exposed to these toxic materials. Toxic material that animals or plants are exposed to will break down only after a long time. Fossil fuels must be burned to obtain energy from them. In the combustion process, particles, such as dust and other pollutants, will be released into the atmosphere. The main exemptions include sulfur, nitrogen, and carbon in which the release of these particles will pollute and harm the environment and the atmosphere. These particles can combine with water particles in the air to form the acid component of acid rain. Fossil fuel combustion also releases high amounts of carbon dioxide into the air. Carbon dioxide emissions increase the greenhouse effect, and the greenhouse effect is the main reason for climate change.

Considering the aforementioned energy crises and environmental

* Corresponding author.
E-mail addresses: a.fudholi@gmail.com, a.fudholi@ukm.edu.my (A. Fudholi).

https://doi.org/10.1016/j.solener.2017.11.056
Received 15 November 2016; Received in revised form 7 November 2017; Accepted 21 November 2017
0038-092X/ © 2017 Elsevier Ltd. All rights reserved.

Nomenclature

A	area (m^2)
C	specific heat of air (J/kg °C)
G	solar radiation (W/m^2)
h	heat transfer coefficient (W/m^2 °C)
H	collector height (m)
k	thermal conductivity (W/m °C)
L	length of collector plate (m)
$\dot{m}$	mass flow rate (kg/s)
R_e	Reynolds number
P_r	Prandtl number
W	width of the collector
T	temperature (°C)
U_b	collector back loss coefficient (W/m^2 °C)
U_t	collector top loss coefficient (W/m^2 °C)

Greek symbols

ε	emissivity
σ	Stefan-Boltzmann constant
τ	Transmission coefficient
α	absorption coefficient
μ	dynamic viscosity
η	efficiency

Subscripts

1 and 2	referred to first and second stream
a	ambient
b	back plate
c	convection; collector
f	fluid
i	inlet
o	outlet
p	photovoltaic
r	radiative
s	sky
w	wind

issues, many developing countries have been committing to take advantage of renewable energy. Solar energy is a renewable energy that can generate electricity via photovoltaic (PV) module and produce heat via a thermal system. Photovoltaic thermal (PVT) collector is based on an integrated system in which electrical and thermal energies are simultaneously produced (Kumar and Rosen, 2011).

A mathematical model is an investigation tool that explores the behavior and characteristics of PVT systems in virtual environments. A mathematical model will facilitate the calculation of energy production, either electrical or thermal, from the PVT system under changing environmental conditions (Hasan and Parida, 2016). The mathematical models adopting hybrid performance analysis of air-based PVT collectors are explored. Comparison of models shows that Model III, in which air flows above and below the observer plate in a system, has better electrical and thermal performance than the other models (Baskar and Edison, 2013). Dubey et al. (2009) studied the performances of a PVT with a hybrid air-based collector under four different configurations.

Jin et al. (2010) studied the performances of PVT collectors with and without a rectangle tunnel absorber. They reported that PVT efficiency was higher for a PVT collector with a rectangle tunnel absorber than that without a rectangle tunnel absorber, and electrical efficiency increased when the PV panel was cooled by air flow. Chow et al. (2008) adopted a numerical method approach to study a water-based solar BIPVT collector. Their findings were congruent with the experimental data. Ji et al. (2009) developed a dynamic model of an innovative PVT solar-assisted heat pump system intended to produce heat and electricity. The simulation model and experimental results achieved acceptable predictions. Abdolzahed and Amri (2009) explored the possibility of improving the performance of a PVT water pumping system. They found that the system performances can be significantly enhanced. Santbergen et al. (2010) designed a PVT with water-based solar collector. Numerical simulation estimated thermal and electrical efficiency. Gang et al. (2012) developed a mathematical model of heat-pipe PVT systems under three typical climates in China. The heat-pipe PVT systems were compared with the traditional water-type PVT system. Mishra and Tiwari (2013) performed proportional analysis on a hybrid PVT water collector with two different configurations in which the collector is partially and fully covered by a PV panel. Shan et al. (2013) studied the dynamic performances of PVT water-based solar collector under different climate situations. The effects of design parameters on PV and thermal performance were investigated. Mahjoubi et al. (2014) developed an energy balance model to determine the real-time performance of a PVT water pump system in Tunisia. Experimental and model results were compared with those results in previous studies. Fudholi et al. (2014a) studied the performances of a PVT water collector under different solar radiation points and with changing mass flow rates of air. Hazi et al. (2014) constructed a mathematical model of a PVT system to assess economic pointers and energy factors in different climate positions in Romania.

Many studies have been conducted on solar collectors with the V-groove to determine the required temperature for the drying process. Previous studies showed that the use of V-groove in the solar collector demonstrates higher thermal efficiency. Heat transfer in the solar collector without V-groove only depends on the back surface of the photovoltaic panel. Heat transfer in the solar collector with the V-groove is more efficient because the surface area of heat transfer increased without V-groove using the principles of conduction, convection, and radiation (Elshafei et al., 2010; Parker, 1981; Parker et al., 1993; Karim and Hawlader, 2006a,b). Conductivity is a heat transfer mechanism that is quick and effective.

The V-groove is not used in this study. The V-groove is converted into the ∇-groove. Heat conductivity is expected to be higher than that of the V-groove. Thermal conductivity depends on the surface area of the two materials in contact. A wide contact surface between the two materials will lead to high thermal conductivity. The V-groove that comes into contact with the back of the photovoltaic solar collectors are few, because only V vertices come into contact with the back of the photovoltaic solar collectors. However, the ∇-groove can come into contact with the whole backside of the photovoltaic solar collectors. Heat transfer can be improved. Therefore, ∇-groove is chosen as the heat transfer medium of photovoltaic solar collectors. By contrast, these studies compared the mathematical and experimental PVT analyses with ∇-groove base on energy and exergy analyses with different solar radiations and mass flow rates.

2. Mathematical modeling

The cross-sectional view of the PVT collector with the ∇-groove is shown in Fig. 1 showing various heat transfer coefficients. To write the energy balance equation of the PVT collector, the following assumptions are made: (i) the performance is in steady state; (ii) all convection heat transfer coefficients in the channels and air flowing are equal and constant; (iii) the useful heat gain to air is uniform along the length of the collector and the ohmic losses in the solar cell is negligible.

The steady-state energy balance equations for PVT with ∇-groove are given below:

For PV,

$$\tau\alpha G = U_t(T_p - T_a) + h_1(T_p - T_f) + h_{rpb}(T_p - T_b) + \eta_p G + Q_n \quad (1)$$

For air flow channel,

$$mC(T_o - T_i) = h_1(T_p - T_f) + h_2(T_b - T_f) + Q_n \quad (2)$$

For back plate,

$$h_{rpb}(T_p - T_b) = h_2(T_b - T_f) + U_b(T_b - T_a) \quad (3)$$

where

$$U_b = \frac{k_t}{l_t} \quad (4)$$

$$U_t = \left(\frac{1}{h_w + h_{rpa}}\right)^{-1} \quad (5)$$

$$h_{rpb} = \frac{\sigma(T_p + T_b)(T_p^2 + T_b^2)}{\left(\frac{1}{\varepsilon_p} + \frac{1}{\varepsilon_b} - 1\right)} \quad (6)$$

$$h_{rpa} = \varepsilon_p \sigma (T_p^2 + T_{sky}^2)(T_p - T_{sky}) \quad (7)$$

$$T_{sky} = 0.0522 T_a^{1.5} \quad (8)$$

where ε_p, σ, T_a, T_{sky}, and T_p are the emissivity of PV, Stefan Boltzman constant, ambient, sky, and PV temperature, respectively.

The convective heat transfer coefficients are given as (Fudholi et al., 2013a,b; Ong, 1995):

$$h = \frac{k}{D_h} Nu \quad (9)$$

which

$$D_h = \frac{4Wd}{2(W + d)} \quad (10)$$

where W, d, and D_h are the width, high, equivalence diameter of the channel, respectively; k is the air thermal conductivity; and Nu is the Nusselt number.

The Nusselt numbers are given below for $Re < 2300$ (laminar flow region):

$$Nu = 5.4 + \frac{0.00190\left[RePr\left(\frac{D_h}{L}\right)\right]^{1.71}}{1 + 0.00563\left[RePr\left(\frac{D_h}{L}\right)\right]^{1.17}} \quad (11)$$

For $2300 < Re < 6000$ (transition flow region):

$$Nu = 0.116(Re^{2/3} - 125)Pr^{1/3}\left[1 + \left(\frac{D_h}{L}\right)^{2/3}\right]\left(\frac{\mu}{\mu_w}\right)^{0.14} \quad (12)$$

For $Re > 6000$ (turbulent flow region):

$$Nu = 0.018 Re^{0.8} Pr^{0.4} \quad (13)$$

where Re and Pr are the Reynolds and Prandtl number, respectively, given as:

$$Re = \frac{mD_h}{A_{ch}\mu} \quad (14)$$

$$Pr = \frac{\mu C}{k} \quad (15)$$

The theoretical model assumes for a short collector or that less than 10 m. The mean air temperature is then equal to the arithmetic mean, where:

$$T_f = \frac{(T_i + T_o)}{2} \quad (16)$$

The physical properties of air are (Fudholi et al., 2013a,b; Ong, 1995):

Density

$$\rho = 1.1774 - 0.00359(T - 27) \quad (17)$$

Specific heat

$$C = 1.0057 + 0.000066(T - 27) \quad (18)$$

Thermal conductivity

$$k = 0.02624 + 0.0000758(T - 27) \quad (19)$$

Viscosity

$$\mu = [1.983 + 0.00184(T - 27)]10^{-5} \quad (20)$$

An iterative process is then initiated. Excel calculates all the required HTCs. HTCs are calculated according to the initially predicted temperature values. In this study, air, ambient, PV, and back plate temperatures of the first section were initially predicted and specified, except those of the PV, which was set to 30 °C above the ambient temperature. The back plate and air temperature in the channel were set at 20 °C and 10 °C above the ambient temperature, respectively. The major design parameters are given as $L = 1.2$ m, $W = 0.53$ m, $\alpha = 0.9$, $\tau = 0.92$, $\varepsilon_p = 0.7$, $\varepsilon_b = 0.9$, $T_a = T_i = 27$ °C, and $V = 1$ m/s.

For simplicity, Eqs. (1)–(3) can be presented in a 3 × 3 matrix form.

$$[A][T] = [B] \quad (21)$$

$$\begin{bmatrix} Z_1 & -Z_2 & -h_{rpb} \\ Z_4 & Z_5 & h_2 \\ h_{rpb} & h_2 & Z_7 \end{bmatrix}\begin{bmatrix} T_p \\ T_f \\ T_b \end{bmatrix} = \begin{bmatrix} Z_3 \\ Z_6 \\ Z_8 \end{bmatrix} \quad (22)$$

where

$$Z_1 = U_t + h_1 + h_{rpb} + (NA_n h_c \eta_n) \quad (23)$$

$$Z_2 = h_1 + (NA_n h_c \eta_n) \quad (24)$$

$$Z_3 = \alpha\tau G + U_t T_a - \eta_p G \quad (25)$$

$$Z_4 = h_1 + (NA_n h_c \eta_n) \quad (26)$$

$$Z_5 = -[h_1 + h_2 + 2mC + (NA_n h_c \eta_n)] \quad (27)$$

$$Z_6 = -2mCT_i \quad (28)$$

$$Z_7 = -(h_2 + h_{rpb} + U_b) \quad (29)$$

$$Z_8 = -U_b T_a \quad (30)$$

$$Q_n = NA_n h_c \eta_n (T_p - T_f) \quad (31)$$

$$\eta_n = \frac{\tanh MH}{MH} \quad (32)$$

$$M = \left(\frac{2h_c l}{k_n A_{cn}}\right)^{1/2} \quad (33)$$

$$h_1 = h_2 = h_c \quad (34)$$

In Eq. (22), the temperature vector may be calculated with Excel by matrix inversion form

$$[T] = [A]^{-1}[B] \quad (35)$$

A standard matrix inversion subroutine is then called to invert $[A]^{-1}$ to calculate a new set of temperature matrix [T′]. Each new temperature value in the matrix [T′] is then compared with the corresponding initially predicted [T]. If the difference between any corresponding new and old values is less than 0.001 °C, the iteration is stopped, and the old temperatures are then replaced with the newly calculated ones and taken to be the required temperatures at the section concerned. In this study, sufficient convergence for T_p, T_f, and T_b was achieved in three to four iterations. Outlet temperature was obtained using Eq. (16).

3. Energy and exergy analysis

Performances of PVT air collectors are characterized by air temperature and thermal and electrical efficiencies. The electrical efficiency of the PV panel depends on its temperature, which corresponds to the cooling performance. Cooling is a feature that distinguishes a PV panel from a PVT collector. Normally, the performances of a PVT air collector is presented by thermal, electrical, and combined efficiencies, which are functions of parameters, such as solar radiation, mass flow rate, ambient, and inlet and outlet temperatures.

The thermal energy efficiency of a PVT air collector is given as

$$\eta = \frac{mC(T_o - T_i)}{AG} \tag{36}$$

where A is the area of the collector, C is the specific heat of the fluid, m is mass flow rate, G is the solar radiation, and T_o and T_i are outlet and inlet temperatures, respectively.

The electrical efficiency of the PVT air collector can be calculated as

$$\eta_p = \eta_0[1 - 0.0045(T_p - 25)] \tag{37}$$

Exergy analysis is based on the second law of thermodynamics, whose effects are due to kinetic and potential energy changes that are neglected; the general exergy rate balance is expressed as (Agrawal and Tiwari, 2011; Ibrahim et al., 2014):

$$\sum \dot{E}x_{in} - \sum \dot{E}x_o = \sum \dot{E}x_d \tag{38}$$

or

$$\sum \dot{E}x_{in} - \sum (\dot{E}x_{th} + \dot{E}x_{PV}) = \sum \dot{E}x_d \tag{39}$$

where

$$\dot{E}x_{in} = A_c N_c G\left[1 - \frac{4}{3}\left(\frac{T_a}{T_s}\right) + \frac{1}{3}\left(\frac{T_a}{T_s}\right)^4\right] \tag{40}$$

$$\dot{E}x_{th} = mC(T_o - T_i)\left(1 - \frac{T_a + 273}{T_o + 273}\right) \tag{41}$$

$$\dot{E}x_{PV} = \eta A_c G \tag{42}$$

$$\dot{E}x_{PVT} = \dot{E}x_{th} + \dot{E}x_{PV} \tag{43}$$

where $\dot{E}x_{in}$ is the input exergy rate (radiation exergy rate), $\dot{E}x_o$ is the output exergy rate, $\dot{E}x_{th}$ is the thermal exergy rate, $\dot{E}x_{PVT}$ is the photovoltaic thermal exergy rate, A_c is the collector area, N_c is the collector's number, G is the solar radiation, T_a is the ambient temperature, and T_s is the sun temperature ($T_s = 5777$ K).

The exergy loss rate and second law of efficiency is expressed as

$$\dot{E}x_{loss} = \dot{E}x_d = \dot{E}x_{in} - \dot{E}x_o \tag{44}$$

$$\eta_{ex} = \frac{\dot{E}x_o}{\dot{E}x_{in}} \tag{45}$$

Van Gool (1997) proposed that maximum improvement in the exergy efficiency for a system or process is achieved when exergy destruction rate ($\dot{E}x_d$) is minimized. He suggested that employing the concept of an exergetic "improvement potential (IP)" is useful when analyzing different processes or sectors of the economy (Akpinar, 2010). The IP of a system or process is expressed as (Fudholi et al., 2015, 2014b,c, 2013a; Ibrahim et al., 2014):

$$IP = (1 - \eta_{ex})\dot{E}x_d \tag{46}$$

where η_{ex} is the second law efficiency.

4. Material and method

An experimental setup and an indoor testing facility of the PVT collector with ∇-groove is shown in Fig. 2. The solar simulator used 23 halogen lamps (500 W in each lamp). The PVT collector consists of a PV panel, ∇-groove, insulator, and blower. The ∇-groove acted as an absorber and was located at the back side of the 80 W PV panel. The ∇-groove is produced in the form of a rod or a total of 13 units of the ∇-groove. The length of each ∇-groove is 114 cm, and each vertex angle of the ∇-groove is 60°. The length and height of each side of the ∇-groove is 3.45 and 3.5 cm, respectively (Fig. 3). The tunnel bars were placed at the back surface of the PV panel. The PV panel was insulated with polyethylene. Regulators were used to control the solar radiation or the brightness of the solar simulator. Ducting was used to connect a blower to the PVT with the ∇-groove.

The experiments were performed to evaluate thermal performance

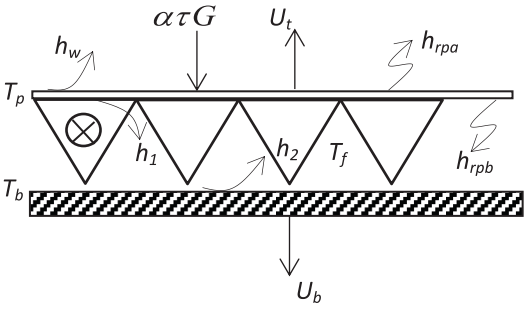


Fig. 1. Schematic diagram of heat transfer characteristics (HTCs) in a PVT air collector.



Fig. 2. Photograph of PVT collector with ∇-groove under solar simulator.



Fig. 3. Photograph of PVT collector with ∇-groove.

Table 1
Uncertainties in the measurements of the parameters.

Parameters	Unit	Uncertainty Comment
Outlet temperature	°C	± 0.24
Inlet temperature	°C	± 0.24
Ambient temperature	°C	± 0.24
Air velocity	m/s	± 0.2
Solar radiation	W/m^2	± 0.4

under two different solar radiation values. Solar radiation from the solar simulator was set to 385 and 820 W/m^2. Each solar radiation was tested under five different mass flow rates, ranging from 0.007 to 0.07 kg/s. Data were collected to calculate thermal and electrical efficiencies. The multimeter was used to collect data, such as voltage, current, and temperature. An air flow DTA 4000 anemometer was used to determine the air flow velocity in the PVT system. A pyranometer was used to determine solar radiation and J-type thermocouples connected to the multimeter.

Uncertainties and errors in the experiments can arise from instrument selection, condition, calibration, reading, environmental factors, and observation. In the experiments, the temperature, air velocity, and solar radiation were measured with appropriate instruments. During the measurements of the parameters, the uncertainties that occurred are shown in Table 1. The estimation of uncertainties was calculated by El-Sebaii et al. (2011).

$$X_R = [(x_1)^2 + (x_2)^2 + ...(x_n)^2]^{1/2} \quad (47)$$

where

X_R = uncertainty in result
$x_1, x_2 ... x_n$ = uncertainty in the independent variables.

The accuracy of the estimation results was calculated (Fudholi et al., 2013a; Ho et al., 2005):

$$E = \frac{1}{n}\sum_{j=1}^{n}\frac{|\hat{\eta}_j - \eta_j|}{\hat{\eta}_j} \quad (48)$$

where $\hat{\eta}_j$ are the experimental value, and η_j and n are theoretical value and the number of experiments, respectively.

5. Result and discussion

A mathematical model for predicting the thermal efficiency of a PVT collector with ∇-groove was conducted. Experimental results was compared with the mathematical model through steady-state investigation. Results indicated the effects of different solar radiations and mass flow rates on the thermal efficiency and temperature of a PVT collector with ∇-groove.

Figs. 4 and 5 show the PV temperature and outlet temperature, which were obtained from the mathematical model (theoretical) and experimental results. Fig. 4 shows the PV and outlet temperature distribution of the PVT collector with ∇-groove at solar radiation of 385 W/m^2. Fig. 5 shows the PV and output temperature distribution at solar radiation of 820 W/m^2. From Figs. 4 and 5, it is clear that by increasing the mass flow rate simultaneously dropped the temperatures (T_p and T_o) of the PVT collector with ∇-groove for both the solar radiations as more and more air volume is available to take away heat from the channel walls hence decreasing PV temperature. The outlet temperature also reduces with increasing air flow rate since the air velocity in the channel is increased hence air has less time inside the channel to attain higher outlet temperatures.

Table 2 shows the results of the outlet and PV temperatures of the PVT collector with ∇-groove. The mathematical model was validated through comparison with the experimental results. The mathematical

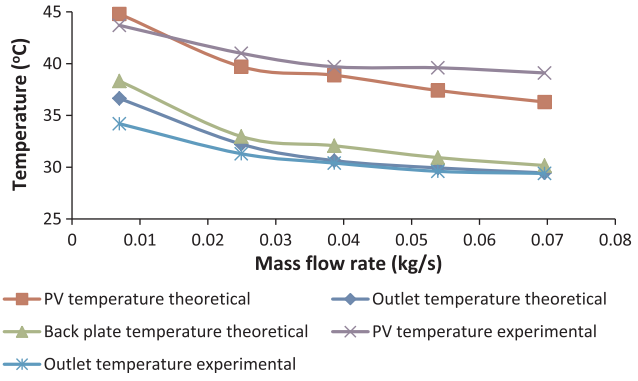


Fig. 4. Theoretical and experimental results of the PVT collector with ∇-groove under 385 W/m^2 solar radiation.

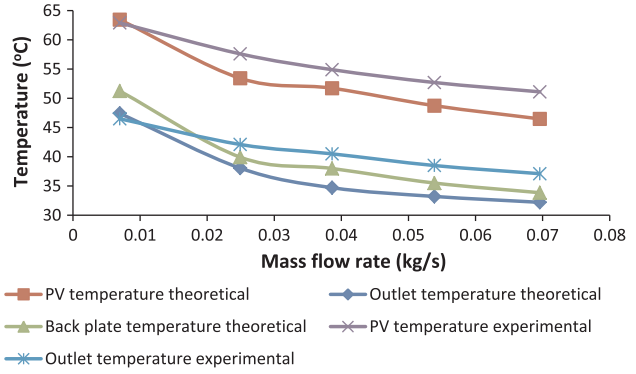


Fig. 5. Theoretical and experimental results of the PVT collector with ∇-groove under 820 W/m^2 solar radiation.

Table 2
Comparison of theoretical and experimental studies for outlet and PV temperature of PVT collector.

m (kg/s)	G (W/m^2)	PV temperature, T_p (°C)			Outlet temperature, T_o (°C)		
		Theo.	Exp.	% error	Theo.	Exp.	% error
0.00696	385	44.8	43.7	2.5	36.6	34.2	6.6
	820	63.5	62.9	0.9	47.4	46.5	1.9
0.02492	385	39.7	41	3.3	32.2	31.3	2.8
	820	53.4	57.6	7.9	38.1	42.1	10.5
0.03861	385	38.9	39.7	2.1	30.6	30.4	0.7
	820	51.7	54.9	6.2	34.7	40.5	16.7
0.05387	385	37.4	39.6	5.9	29.9	29.6	1.0
	820	48.7	52.7	8.2	33.2	38.5	16.0
0.06958	385	36.3	39.1	7.7	29.5	29.4	0.3
	820	46.5	51.1	9.9	32.2	37.1	15.2
Average				**5.4**			**7.2**

model presented fair predictions with an average error of 5.4% and 7.2% for PV and outlet temperature, respectively. Mathematical model results are consistent with the experimental data with accuracy of 94.6% and 92.8% for PV and outlet temperature, respectively.

Figs. 6 and 7 show the energy efficiency versus the mass flow rate of PVT collector with ∇-groove. The PVT and thermal efficiencies of PVT collector with ∇-groove increases with increasing mass flow rate of air. Table 3 shows the corroboration of the mathematical model results and experimental data. Mathematical model results are consistent with the experimental data with an accuracy of 91.3% for PVT efficiency. By contrast, the results on PV and thermal efficiencies revealed that the mathematical model and the experimental data had accuracy of 98.59% and 89%, respectively.

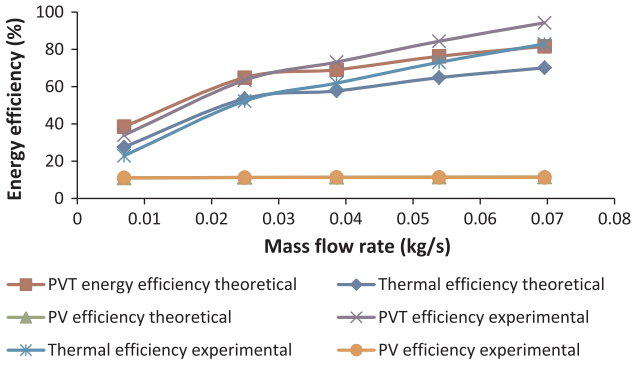


Fig. 6. Energy efficiency versus mass flow rate under 385 W/m^2 solar radiation.

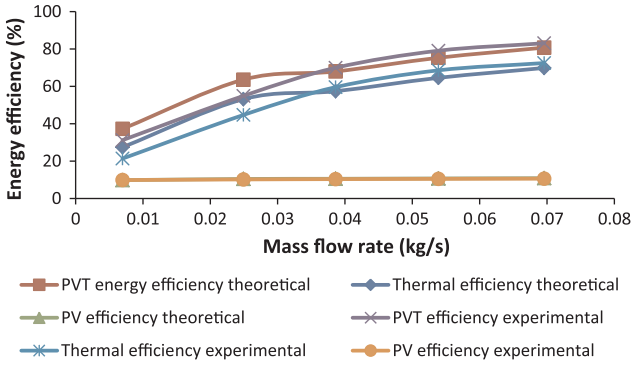


Fig. 7. Energy efficiency versus mass flow rate under 820 W/m^2 solar radiation.

Fig. 8 shows the graphs of the temperature difference ($T_o - T_i$) versus the mass flow rate of air from the theoretical study. The mass flow rate of air is the same as that ranges from 0.006 to 0.069 kg/s for radiations of 300 to 1000 W/m^2. $T_o - T_i$ is the temperature between the inlet temperature to the solar collector, and the temperature goes out of the solar collector. $T_o - T_i$ also means that the temperature in the solar collector is successfully absorbed by air and taken out of the collector. Fig. 8 shows that $T_o - T_i$ decreases when the mass flow rate of air is rising for various solar radiations because air flows stronger into the accumulator when the mass flow rate of air increases. By contrast, for solar radiations of 300–1000 W/m^2, thermal efficiency increases when the mass flow rate of air is rising, as shown in Tables 4–8. Additionally, these tables show the value of PV and PVT efficiencies, T_p, T_b, T_f, T_o, and $T_o - T_i$. Fig. 9 shows that PV efficiency increases when the mass flow rate and PV temperature decrease.

Figs. 10 and 11 show the exergy analysis of PVT collector with

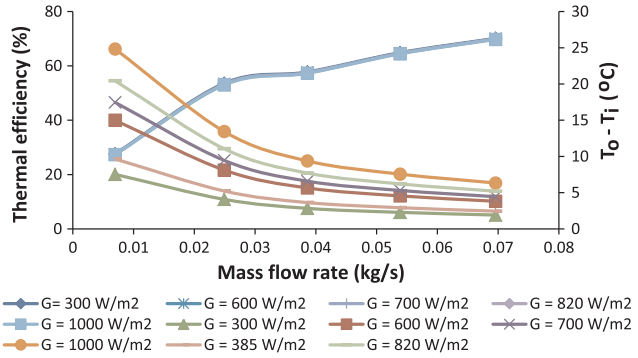


Fig. 8. Temperature difference ($T_o - T_i$) and thermal efficiency versus mass flow rate for various solar radiations from theoretical results (energy analysis).

Table 4
Theoretical result for temperatures and efficiencies from energy analysis under mass flow rate of 0.00696 kg/s.

G	Efficiency (%)			Temperature (°C)				
(W/m^2)	PV	Thermal	PVT	T_p	T_b	T_f	T_o	$T_o - T_i$
300	11.2	27.6	38.8	41.0	35.8	30.8	34.5	7.5
385	11.0	27.6	38.6	44.8	38.3	31.8	36.6	9.6
500	10.7	27.5	38.2	49.9	41.7	33.3	39.5	12.5
600	10.4	27.5	37.9	54.2	44.7	34.5	42.0	15.0
700	10.1	27.5	37.6	58.4	47.7	35.7	44.5	17.5
820	9.8	27.4	37.3	63.5	51.3	37.2	47.4	20.4
900	9.6	27.4	37.0	66.7	53.6	38.2	49.4	22.4
1000	9.4	27.3	36.7	70.8	56.6	39.4	51.8	24.8
1200	8.9	27.2	36.1	78.6	62.5	41.8	56.7	29.7
Average	**10.1**	**27.5**	**37.6**					

∇-groove. The PVT exergy efficiency has a similar trend, rises slowly, and tends to be constant for both theoretical and experimental studies, which were produced PVT exergy efficiencies of 11.72–13.26% with an average of 12.79%. In the theoretical study, exergy loss rate is 198–198.9 W and 421–425 W with an average of 198.4 and 422.8 W for solar radiations of 385 and 820 W/m^2, respectively. In the experimental study, exergy loss rate is 198.5–199.5 W and 421.6–428.1 W with an average of 198.8 and 423.5 W for solar radiation of 385 and 820 W/m^2, respectively. At the solar radiation of 385 W/m^2, the PVT air collector with ∇-groove produced IPs of 172–173.6 W and 173–174.7 W with an average of 172.7 and 173.4 W for theoretical and experimental studies, respectively. At a solar radiation of 820 W/m^2, the PVT air collector with ∇-groove produced IPs of 365.2–372.1 W and 366.5–377.9 W with an average of 368.2 and 369.9 W for theoretical and experimental

Table 3
Comparison of theoretical and experimental results for PV, thermal, and PVT efficiencies based on energy analysis results.

M (kg/s)	G (W/m^2)	PV efficiency (%)			Thermal efficiency (%)			PVT efficiency (%)		
		Theo.	Exp.	Error	Theo	Exp.	Error	Theo.	Exp.	Error
0.00696	385	10.99	11.05	0.62	27.6	22.9	17.1	38.57	33.92	12.04
	820	9.83	9.87	0.35	27.4	21.3	22.2	37.26	31.21	16.25
0.02492	385	11.30	11.22	0.71	53.5	52.2	2.5	64.82	63.43	2.15
	820	10.45	10.19	2.47	53.1	44.7	15.9	63.60	54.89	13.70
0.03861	385	11.35	11.30	0.45	57.7	61.9	7.2	69.05	73.16	5.96
	820	10.56	10.36	1.86	57.4	59.6	3.8	67.97	69.94	2.90
0.05387	385	11.44	11.31	1.19	64.8	73.0	12.7	76.26	84.34	10.59
	820	10.74	10.50	2.28	64.6	68.6	6.2	75.30	79.08	5.02
0.06958	385	11.51	11.34	1.51	70.1	82.9	18.3	81.61	94.24	15.48
	820	10.88	10.60	2.63	69.8	72.5	3.8	80.73	83.07	2.90
Average				1.41			**11.0**			**8.70**

Table 5
Theoretical result for temperatures and efficiencies from energy analysis under mass flow rate of 0.02492 kg/s.

G	Efficiency (%)			Temperature (°C)				
(W/m^2)	PV	Thermal	PVT	T_p	T_b	T_f	T_o	$T_o - T_i$
300	11.5	53.6	65.1	37.0	31.6	29.0	31.1	4.1
385	11.3	53.5	64.8	39.7	33.0	29.6	32.2	5.2
500	11.1	53.4	64.5	43.4	34.8	30.4	33.8	6.8
600	10.9	53.3	64.2	46.6	36.4	31.1	35.1	8.1
700	10.7	53.2	63.9	49.7	38.0	31.7	36.5	9.5
820	10.5	53.1	63.6	53.4	39.9	32.5	38.1	11.1
900	10.3	53.1	63.4	55.9	41.2	33.1	39.1	12.1
1000	10.1	53.0	63.1	58.9	42.9	33.7	40.4	13.4
1200	9.7	52.8	62.5	64.9	46.2	35.0	43.1	16.1
Average	**10.7**	**53.2**	**63.9**					

Table 6
Theoretical result for temperatures and efficiencies from energy analysis under mass flow rate of 0.03861 kg/s.

G	Efficiency (%)			Temperature (°C)				
(W/m^2)	PV	Thermal	PVT	T_p	T_b	T_f	T_o	$T_o - T_i$
300	11.5	57.8	69.3	36.3	30.9	28.4	29.8	2.8
385	11.4	57.7	69.0	38.9	32.1	28.8	30.6	3.6
500	11.1	57.6	68.8	42.3	33.6	29.4	31.7	4.7
600	11.0	57.5	68.5	45.3	35.0	29.8	32.7	5.7
700	10.8	57.5	68.3	48.2	36.3	30.3	33.6	6.6
820	10.6	57.4	68.0	51.7	38.0	30.9	34.7	7.7
900	10.4	57.3	67.8	54.0	39.1	31.2	35.5	8.5
1000	10.2	57.3	67.5	56.9	40.5	31.7	36.4	9.4
1200	9.9	57.1	67.0	62.5	43.3	32.6	38.2	11.2
Average	**10.8**	**57.5**	**68.2**					

Table 7
Theoretical result for temperatures and efficiencies from energy analysis under mass flow rate of 0.05387 kg/s.

G	Efficiency (%)			Temperature (°C)				
(W/m^2)	PV	Thermal	PVT	T_p	T_b	T_f	T_o	$T_o - T_i$
300	11.6	64.9	76.5	35.1	30.0	28.1	29.3	2.3
385	11.4	64.8	76.3	37.4	30.9	28.5	29.9	2.9
500	11.3	64.7	76.0	40.4	32.1	28.9	30.8	3.8
600	11.1	64.7	75.8	43.1	33.2	29.3	31.6	4.6
700	10.9	64.6	75.6	45.7	34.2	29.7	32.3	5.3
820	10.7	64.6	75.3	48.7	35.5	30.1	33.2	6.2
900	10.6	64.5	75.1	50.8	36.4	30.4	33.8	6.8
1000	10.5	64.4	74.9	53.3	37.4	30.8	34.6	7.6
1200	10.2	64.3	74.4	58.3	39.6	31.5	36.1	9.1
Average	**10.9**	**64.6**	**75.5**					

studies, respectively, as shown in Table 9. The present study is compared with previous studies as shown in Table 10.

6. Conclusion

A mathematical model approach to calculate the performances of PVT collector with ∇-groove compared with experimental results was presented. A matrix inversion method was adopted to solve the temperature equation for each PVT system element. Mathematical model results are consistent with experimental data with accuracy of approximately 94%. The average PVT energy efficiency is 65.52% and 66.73% for theoretical and experimental studies, respectively. The average PVT exergy efficiency is 12.91% and 12.66% for theoretical and experimental studies, respectively. The average IP is 173 and

Table 8
Theoretical result for temperatures and efficiencies from energy analysis under mass flow rate of 0.06958 kg/s.

G	Efficiency (%)			Temperature (°C)				
(W/m^2)	PV	Thermal	PVT	T_p	T_b	T_f	T_o	$T_o - T_i$
300	11.6	70.1	81.8	34.3	29.5	28.0	28.9	1.9
385	11.5	70.1	81.6	36.3	30.2	28.2	29.5	2.5
500	11.3	70.0	81.4	39.0	31.1	28.6	30.2	3.2
600	11.2	70.0	81.2	41.4	32.0	28.9	30.8	3.8
700	11.1	69.9	81.0	43.7	32.8	29.2	31.4	4.4
820	10.9	69.8	80.7	46.5	33.9	29.6	32.2	5.2
900	10.8	69.8	80.6	48.3	34.5	29.9	32.7	5.7
1000	10.6	69.7	80.4	50.6	35.4	30.2	33.3	6.3
1200	10.3	69.6	80.0	55.1	37.2	30.8	34.6	7.6
Average	**11.0**	**69.9**	**80.9**					

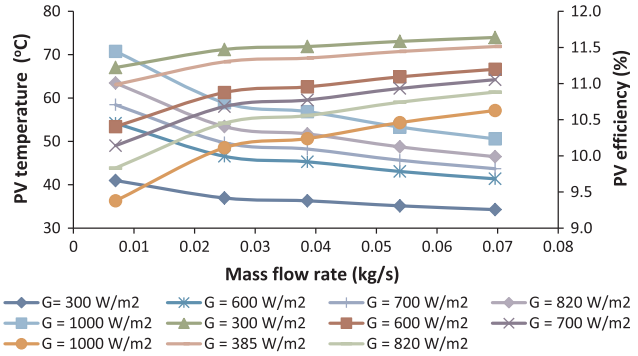


Fig. 9. PV temperature and PV efficiency versus mass flow rate for various solar radiations from energy analysis.

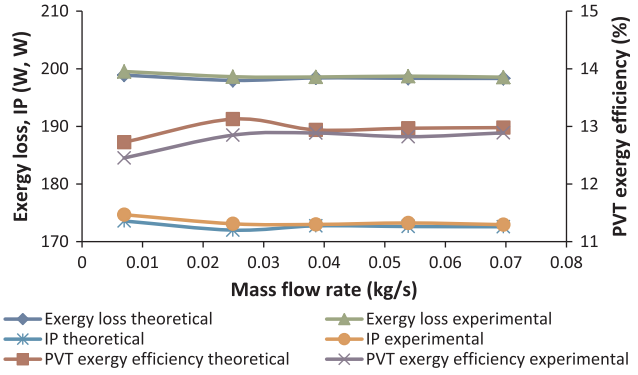


Fig. 10. Variation of exergies and exergy efficiencies under a mass flow rate of 385 W/m^2.

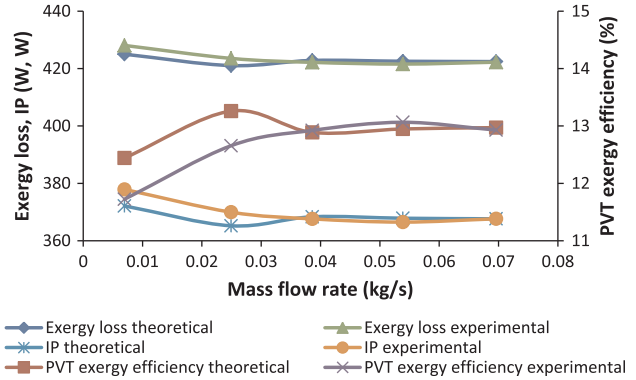


Fig. 11. Variation of exergies and exergy efficiencies under a mass flow rate of 820 W/m^2.

Table 9
Exergy analysis of the PVT air collector with V-groove.

m (kg/s)	S (W/m^2)	PVT exergy efficiency (%)			Exergy loss (W)			IP (W)		
		Theo.	Exp.	% error	Theo.	Exp.	% error	Theo.	Exp.	% error
0.00696	385	12.73	12.45	2.15	198.90	199.53	0.31	173.6	174.7	0.63
	820	12.44	11.72	5.78	425.02	428.08	0.72	372.1	377.9	1.52
0.02492	385	13.13	12.85	2.12	197.99	198.62	0.32	172.0	173.1	0.64
	820	13.26	12.66	4.55	421.05	423.56	0.59	365.2	370.0	1.28
0.03861	385	12.94	12.89	0.42	198.42	198.58	0.08	172.7	173.0	0.14
	820	12.89	12.92	0.27	422.85	422.18	0.16	368.4	367.6	0.20
0.05387	385	12.97	12.82	1.13	198.35	198.72	0.19	172.6	173.2	0.35
	820	12.95	13.06	0.90	422.56	421.58	0.23	367.8	366.5	0.37
0.06958	385	12.98	12.89	0.70	198.33	198.54	0.11	172.6	173.0	0.21
	820	12.97	12.93	0.33	422.45	422.23	0.05	367.7	367.6	0.00
Average				**1.84**			**0.28**			**0.53**

Table 10
Comparison of the present study of energy and exergy analyses.

Method and results	PVT Efficiency (%)		References
	Energy	Exergy	
Theoretical (T) and experimental (E) η_{PV} = 8.4%, η_{th} = 42%	50.4		Solanki et al. (2009)
T: η_{th} = 34–70%; η_{PV} = 3.7–4.3%	T: 37.7–74.3		Othman et al. (2007)
E: η_{th} = 33–71%; η_{PV} = 1.8–2.1%	E: 34.8–73.1		
T: η_{PV} = 10%, η_{th} = 17.2%	45	10.75	Sarhaddi et al. (2010a)
T: η_{PV} = 9.5–11%, η_{th} = 7–21%, η_{PVT} = 45%	38–48		Sarhaddi et al. (2010b)
E: η_{PV} = 12.4%, η_{th} = 35.7%	48.1		Agrawal et al. (2012)
T: η_{PV} = 14–15%	55–65	12–15	Joshi and Tiwari (2007)
E & T: η_{PV} = 9.5–11%, η_{th} = 39–46%, η_{th} = 26.4–30.5% (thermal equivalent of electrical efficiency)	65.4–76.5		Joshi et al. (2009)
E & T		4	Nayak and Tiwari (2008)
	55	13.5	Bosanac et al. (2003)
E & T	T: 38.8–81.8	E: 11.72–13.06	Present study
	E: 31.2–94.2	T: 12.44–13.26	

369 W for solar radiations of 385 and 820 W/m^2, respectively. For energy analysis, the effect of solar radiation on efficiency is small, and mass flow rate significantly affects efficiency. For exergy analysis, solar radiation and mass flow rate has minimal effect on PVT exergy efficiency.

Acknowledgments

The authors would like to thank the Ministry of Higher Education, Malaysia for funding (FRGS/1/2014/ST02/UKM/03/1) and UKM for funding (GGPM-2014-029), also the Solar Energy Research Institute (SERI), UKM for providing the laboratory facilities and technical support.

References

Agrawal, S., Tiwari, G.N., Pandey, H.D., 2012. Indoor experimental analysis of glazed hybrid photovoltaic thermal tiles air collector connected in series. Energy Build. 53, 145–151.
Agrawal, S., Tiwari, G.N., 2011. Energy and exergy analysis of hybrid micro-channel photovoltaic thermal module. Sol. Energy 85, 356–370.
Akpinar, E.K., 2010. Drying of mint leaves in solar dryer and under open sun: modeling, performance analyses. Energy Convers. Manage. 51, 2407–2418.
Baskar, P., Edison, G., 2013. A review of mathematical models for performance analysis of hybrid solar photovoltaic – thermal (PV/T) air heating systems. Adv. Mater. Res. 768, 29–39.
Bosanac, M., Sorensen, B., Katic, I., Sorensen, H., Nielsen, B., Badran, J., 2003. Photovoltaic/Thermal Solar Solar Collectors and Their Potential in Denmark. Danish Technological Institute, Solar Energy Centre.
Chow, T.T., He, W., Chan, A.L.S., Fong, K.F., Lin, Z., Ji, J., 2008. Computer modeling and experimental validation of a building-integrated photovoltaic and water heating system. Appl. Therm. Eng. 28 (11–12), 1356–1364. http://dx.doi.org/10.1016/j.applthermaleng.2007.10.007.
Dubey, S., Sandhu, G.S., Tiwari, G.N., 2009. Analytical expression for electrical efficiency of PV/T hybrid air collector. Appl. Energy 86 (5), 697–705. http://dx.doi.org/10.1016/j.apenergy.2008.09.003.
El-Sebaii, A.A., Aboul-Enein, S., Ramadan, M.R.I., Shalaby, S.M., Moharram, B.M., 2011. Thermal performance investigation of double pass finned plate solar air heater. Appl. Energy 88, 1727–1739.
Elshafei, E.A.M., Awad, M.M., El-Negiry, E., Ali, A.G., 2010. Heat transfer and pressure drop in corrugated channels. Energy 35 (1), 101–110.
Fudholi, A., Sopian, K., Alghoul, M.A., Ruslan, M.H., Othman, M.Y., 2015. Performance and improvement potential of solar drying system for palm oil fronds. Renew. Energy 78, 561–565.
Fudholi, A., Sopian, K., Yazdi, M.H., Ruslan, M.H., Ibrahim, A., Kazem, H.A., 2014a. Performance analysis of photovoltaic thermal (PVT) water collectors. Energy Convers. Manage. 78, 641–651. http://dx.doi.org/10.1016/j.enconman.2013.11.017.
Fudholi, A., Sopian, K., Yazdi, M.H., Ruslan, M.H., Gabbasa, M., Kazem, H.A., 2014b. Performance analysis of solar drying system for red chili. Sol. Energy 99, 47–54.
Fudholi, A., Sopian, K., Othman, M.Y., Ruslan, M.H., 2014c. Energy and exergy analyses of solar drying system of red seaweed. Energy Build. 68, 121–129.
Fudholi, A., Sopian, K., Othman, M.Y., Ruslan, M.H., Bakhtyar, B., 2013a. Energy analysis and improvement potential of finned double-pass solar collector. Energy Convers. Manage. 75, 234–240.
Fudholi, A., Sopian, K., Ruslan, M.H., Othman, M.Y., 2013b. Performance and cost benefit analysis of double-pass solar collector with and without fins. Energy Convers. Manage. 76, 8–19.
Gang, P., Huide, F., Jie, J., Tin-Tai, C., Tao, Z., 2012. Annual analysis of heat pipe PV/T systems for domestic hot water and electricity production. Energy Convers. Manage. 56, 8–21. http://dx.doi.org/10.1016/j.enconman.2011.11.011.
Greenhalgh, R., 2002. Fossil fuel and its impact on the environment. < http://www.w3.org/TR/1999/REC-html401-19991224/loose.dtd > (29 January 2008).
Hasan, M.A., Parida, S.K., 2016. An overview of solar photovoltaic panel modeling based on analytical and experimental viewpoint. Renew. Sustain. Energy Rev. 60, 75–83.

http://dx.doi.org/10.1016/j.rser.2016.01.087.
Hazi, A., Hazi, G., Grigore, R., Vernica, S., 2014. Opportunity to use PVT systems for water heating in industry. Appl. Therm. Eng. 63 (1), 151–157. http://dx.doi.org/10.1016/j.applthermaleng.2013.11.010.
Ho, C.D., Yeh, H.M., Wang, R.C., 2005. Heat-transfer enhancement in double-pass flat-plate solar air heaters with recycle. Energy 30, 2796–2817.
Ibrahim, A., Fudholi, A., Sopian, K., Othman, M.Y., Ruslan, M.H., 2014. Efficiencies and improvement potential of building integrated photovoltaic thermal (BIPVT) system. Energy Convers. Manage. 77, 527–534.
Ji, J., He, H., Chow, T., Pei, G., He, W., Liu, K., 2009. Distributed dynamic modeling and experimental study of PV evaporator in a PV/T solar-assisted heat pump. Int. J. Heat Mass Transf. 52 (5–6), 1365–1373. http://dx.doi.org/10.1016/j.ijheatmasstransfer.2008.08.017.
Jin, G.L., Ibrahim, A., Chean, Y.K., Daghigh, R., Ruslan, M.H., Mat, S., Othman, M.Y., Sopian, K., 2010. Evaluation of single-pass photovoltaic-thermal air collector with rectangle tunnel absorber. Am. J. Appl. Sci. 7 (2), 277–282.
Joshi, A.S., Tiwari, A., 2007. Energy and exergy efficiencies of a hybrid photovoltaic-thermal (PV/T) air collector. Renew. Energy 32, 2223–2241.
Joshi, A.S., Tiwari, A., Tiwari, G.N., Dincer, I., Reddy, B.V., 2009. Performance evaluation of a hybrid photovoltaic-thermal (PV/T) (glass-to-glass) system. Int. J. Therm. Sci. 48, 154–164.
Karim, M.A., Hawlader, M.N.A., 2006a. Performance evaluation of a v-groove solar air collector for drying applications. Appl. Therm. Eng. 26 (1), 121–130. http://dx.doi.org/10.1016/j.applthermaleng.2005.03.017.
Karim, MA., Hawlader, MNA., 2006b. Performance investigation of flat plate, v-corrugated and finned air collectors. Energy 31 (4), 452–470.
Kumar, R., Rosen, M.A., 2011. A critical review of photovoltaic-thermal solar collectors for air heating. Appl. Energy 88 (11), 3603–3614. http://dx.doi.org/10.1016/j.apenergy.2011.04.044.
Mahjoubi, A., Mechlouch, R.F., Mahdhaoui, B., Ben Brahim, A., 2014. Real-time analytical model for predicting the cell temperature modules of photovoltaic water pumping systems. Sustain. Energy Technol. Assess. 6, 93–104. http://dx.doi.org/10.1016/j.seta.2014.01.009.
Mishra, R.K., Tiwari, G.N., 2013. Energy and exergy analysis of hybrid photovoltaic thermal water collector for constant collection temperature mode. Sol. Energy 90, 58–67. http://dx.doi.org/10.1016/j.solener.2012.12.022.
Nayak, S., Tiwari, G.N., 2008. Energy and exergy analysis of photovoltaic/thermal integrated with a solar greenhouse. Energy Build. 40 (11), 2015–2021.
Ong, K.S., 1995. Thermal performance of solar air heaters: mathematical model and solution procedure. Sol. Energy 55 (2), 93–109.
Othman, M.Y., Yatim, B., Sopian, K., Bakar, M.N.A., 2007. Performance studies on a finned double-pass photovoltaic-thermal (PV/T) solar collector. Desalination 209, 43–49.
Parker, B.F., 1981. Derivation of efficiency and loss factors for solar air heaters. Sol. Energy 26 (1), 27–32.
Parker, B.F., Lindley, M.R., Colliver, D.G., Murphy, W.E., 1993. Thermal performance of three solar air heaters. Sol. Energy 51 (6), 467–479.
Santbergen, R., Rindt, C.C.M., Zondag, H.A., van Zolingen, R.J.C., 2010. Detailed analysis of the energy yield of systems with covered sheet-and-tube PVT collectors. Sol. Energy 84 (5), 867–878. http://dx.doi.org/10.1016/j.solener.2010.02.014.
Shan, F., Cao, L., Fang, G., 2013. Dynamic performances modeling of a photovoltaic-thermal collector with water heating in buildings. Energy Build. 66, 485–494. http://dx.doi.org/10.1016/j.enbuild.2013.07.067.
Sarhaddi, F., Farahat, S., Ajam, H., Behzadmehr, A., 2010a. Exergetic performance assessment of a solar photovoltaic thermal (PV/T) air collector. Energy Build. 42, 2184–2199.
Sarhaddi, F., Farahat, S., Ajam, H., Behzadmehr, A., Adeli, M.M., 2010b. An improved thermal and electrical model for a solar photovoltaic thermal (PV/T) air collector. Appl. Energy 87, 2328–2339.
Solanki, S.C., Dubey, S., Tiwari, A., 2009. Indoor simulation and testing of photovoltaic thermal (PV/T) air collectors. Appl. Energy 86, 2421–2428.
Van Gool, W., 1997. Energy policy: fairly tales and factualities. In: Soares, O.D.D., Martins da Cruz, A., Costa Pereira, G., Soares, I.M.R.T., Reis, AJPS (Eds.), Innovation and Technology-Strategies and Policies. Kluwer Academic Publishers, Dordrecht, pp. 93–105.